Solid Freeform Fabrication 2018: Proceedings of the 29th Annual International Solid Freeform Fabrication Symposium – An Additive Manufacturing Conference
Reviewed Paper

Volume Effects on the Fatigue Behavior of Additively Manufactured Ti-6Al-4V Parts

Jonathan Pegues[1,2], Michael Roach[3], R. Scott Williamson[3], Nima Shamsaei[1,2*]

[1]*Department of Mechanical Engineering, Auburn University, Auburn, AL 36849*

[2]*National Center for Additive Manufacturing Excellence (NCAME), Auburn University, Auburn, AL 36849*

[3]*Department of Biomedical Materials Science, University of Mississippi Medical Center, Jackson, MS 39216*

**Corresponding author:*

Tel: 334-844-4839

Email: shamsaei@auburn.edu

Abstract

Recent interest to implement additive manufactured parts into structural applications has created a critical need to better understand the fatigue behavior of these parts. Alloys such as Ti-6Al-4V are popular in the aerospace and biomedical industries due to their superior strength to weight ratio and biocompatibility. In these two industries, part sizes can range from very small surgical implants to large structural components, all of which are subjected to cyclic loading conditions. The fatigue behavior of additively manufactured parts may show more sensitivity to part size than their wrought counterparts due to the defects that are inherent to the fabrication process. This research investigates the sensitivity of additively manufactured Ti-6Al-4V parts to volume size by comparing the stress-life fatigue curves of three geometries with increasing gage volumes. Results indicate that additive Ti-6Al-4V parts show reduced fatigue lives because of an increase in surface or near-surface defects.

Keywords: Additive manufacturing, Fatigue behavior, Defects, Fractography

Introduction

Additive manufacturing has become an increasingly popular technique to produce structural parts or components. In particular, additive manufacturing has gained a significant amount of interest in aerospace and biomedical fields with Ti-6Al-4V alloys being prominently used in these industries. The popularity of titanium alloys is due to their high strength to weight ratio, biocompatibility, excellent corrosion resistance, and general weldability. The scale of parts for aerospace and biomedical applications can range from small surgical implants to large structural components. It has been well established that fatigue resistance decreases as part size increase as a result of a higher probability of a large part containing a critical sized defect that can result in early fatigue failure [1], [2]. Considering the defects that are common to additive manufactured (AM) parts, there could be a higher sensitivity to part size than what has been previously observed for traditional wrought materials. This leads to a need to understand how the defects common to additive manufacturing methods such as laser powder bed fusion (L-PBF) affect the fatigue behavior of small parts as well as large parts.

Previous research has shown there could be a size effect on the fatigue behavior of additively manufactured Ti-6Al-4V parts in the as-built condition [3]. This could result from surface roughness in which large diameter parts built diagonally were better able to dissipate heat on the down-skin edge of the sample, leading to lower surface roughness and improved fatigue resistance. Research has also shown that in order to improve the fatigue resistance of AM parts, surface modification must be carried out to reduce the surface discontinuities associated with the highly rough as-built surfaces [4], [5]. Even after machining and polishing of AM parts, defects common to this fabrication process such as lack-of-fusion and porosity have been shown to result in large variation in the fatigue lives for Ti-6Al-4V, especially in the high cycle fatigue regime [6]–[8].

To overcome the issue of defects and their effect on the cyclic behavior, Murakami et al. developed the $\sqrt{area}$ approach in with the maximum stress intensity, $K_{max,}$ is estimated for defects using Equation 1 [9]–[11]. In Equation 1, Y is a shape factor and typically taken as 0.65 for surface cracks and 0.5 for sub-surface cracks, σ_{max} is the peak stress, and $\sqrt{area}$ is the effective area of the defect projected onto the fracture plane. This approach simplifies the shape factor for irregular shaped defects making estimation of K_{max} more practical for wide spread applications.

$$K_{max} = Y\sigma_{max}\sqrt{\pi\sqrt{area}} \qquad (1)$$

The objective of the present research is to determine the crack initiation behavior and its effect on the fatigue lives of three geometries ranging from 81 mm^3 to 184 mm^3 gage volumes. A thorough fractographic analysis is conducted to determine the failure mechanisms for each geometry. The Murakami $\sqrt{area}$ approach is then employed to determine its effectiveness as a predictive tool at capturing the effects of defects on the fatigue behavior of L-PBF Ti-6Al-4V.

Materials and Methods

The three geometries implemented in this study were designed to maintain a constant surface area within the uniform gage section while incrementally increasing the gage volume by 50% as shown in Figure 1. To maintain constant surface area and minimize any effects that may arise from simultaneously increasing/decreasing surface areas, the gage diameters and lengths were adjusted accordingly. This resulted in a diameter range of 3.25 mm for the smallest gage volume geometry (G1_81) to 7.30 mm for the largest gage volume geometry (G3_184). Previous research has shown that as-built Ti-6Al-4V parts with diameters below 6.06 mm are susceptible to early failures compared to larger diameters due to the increased surface roughness of the smaller diameter parts [3]. For the present study, however, the surfaces were machined and polished to limit the detrimental effect of surface roughness.

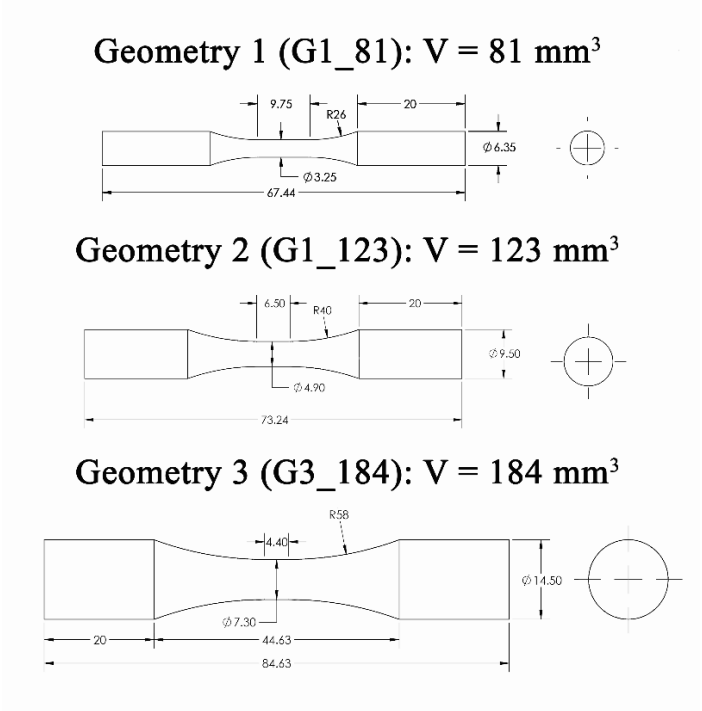

Figure 1: Specimen geometry with all measurements in mm.

Parts were fabricated as cylindrical rods at an angle of 45° from the substrate on an EOS M290 machine. Specimens were machined from the cylindrical rods into the desired geometries and polished using a series of 320 – 4000 grit silicon carbide papers in the longitudinal direction of the gage to remove any horizontal machining marks. Additionally, all specimens were stress relieved before testing to reduce any residual stresses that arise during rapid cooling of the layers during fabrication.

All tests were conducted on an MTS testing frame with a 100 kN capacity under fully reversed (R = -1) force control conditions. All tests were run until failure, after which, fracture

surfaces were carefully removed and prepared for fractography analysis. Fractography was performed on both a Keyence digital microscope and Zeiss-FEG scanning electron microscope (SEM). The defects responsible for crack initiation were identified and measured using ImageJ software. Defects were categorized as either surface or sub-surface defects. Sub-surface defects were defined as defects that were at least their own length (defect diameter) away from the surface. Surface cracks, similarly, were defined as any crack that was directly on the surface or less than their own length from the surface.

Experimental Results

Stress-Life (S-N_f) data is presented for each geometry in Figure 2. Implementing a weakest link approach, the slope of the fatigue curves are considered to be constant for each geometry leading to a system of linear equations in which the Basquin values are determined. The curves generated using this approach are shown along with the data in Figure 2. The data shows increasing fatigue resistance for smaller volume geometries with the smallest geometry (G1_81) showing significantly improved fatigue resistance compared to the larger specimens. While there is some improvement in fatigue resistance observed for G2_123 compared to G3_184, the scatter in the data for these geometries suggests that the fatigue curves are not statistically different. Additionally, the largest gage volume specimens (G3_184) shows a lower mean fatigue life at a stress amplitude of 550 MPa compared to 650 MPa, which may account for the difference in Basquin curve positions.

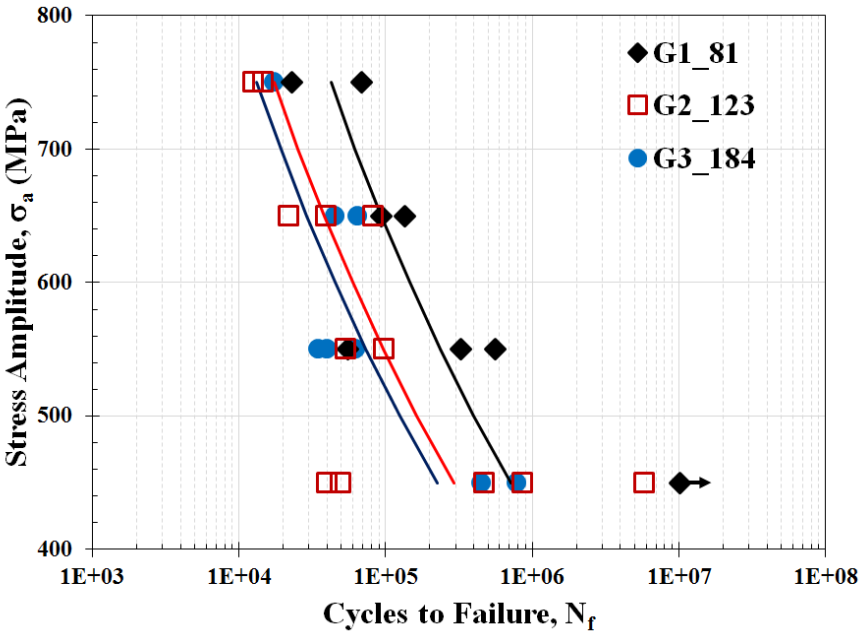

Figure 2: Stress-life data for Geometry 1 (black), Geometry 2 (red), and Geometry 3 (blue).

Interestingly, only G1_81 reached a fatigue limit ($N_f > 10^6$ cycles) at a stress amplitude of 450 MPa. G2_123 showed a surprisingly large range of fatigue lives (50,000 to 5,000,000 cycles) at a stress amplitude of 450 MPa. This large variation in fatigue lives for a similar stress amplitude is most likely related to the crack initiation behavior and the defects common to the L-PBF process. These fatigue curves also indicate that there could be significant differences in the physical defect/crack initiation location or growth between the different geometries, especially G1_81.

Fractography

Fractography analysis revealed an interesting distribution of defects resulting in cracks initiating from both surface and sub-surface defects for both low and high cycle fatigue regimes. This is surprising because fatigue failures are mostly considered to be a surface or near-surface phenomena for the low life regime. Figure 3 shows a representation of sub-surface and surface crack initiation types. All fracture surfaces revealed a single crack which initiated at a pore and propagated until failure, with no evidence of crack coalescence. A small portion of relatively stable crack growth was observed near the initiation site. The tortuosity of the crack then increased, indicating deterioration of the crack stability until fracture. The crack growth areas were surrounded by a typical shear lip associated with final fracture.

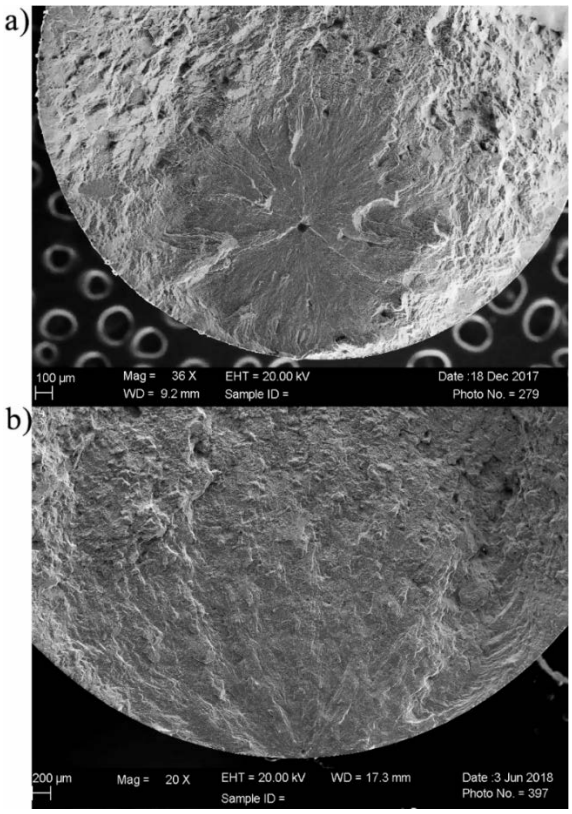

Figure 3: Crack initiation at a surface pore common for a) Geometry 1 and b) Geometry 3.

The pores responsible for crack initiation for G1_81 (smallest gage volume) were mostly located internal to the surface. In contrast, the initiating pores for the two larger gage volume sample types (G2_123 & G3_184) were almost entirely located directly on the surface. All samples showing sub-surface crack initiation resulted in much longer fatigue lives than their surface crack initiation counterparts. Additionally, large surface defects were always associated with the lowest fatigue life for a given geometry and stress amplitude. For example, the shortest fatigue life observed for G2_123 at 450 MPa in Figure 2 had a comparatively large surface defect (d = 78 μm) while the longest at this stress level had much smaller size (d = 25 μm).

The fact that smallest gage volume specimens showed a preference toward subsurface crack initiation explains the separation of the G1_ 81 Basquin curve presented in Figure 2. Additionally, the defects observed for these sub-surface crack initiation sites were much larger than the majority of the surface defects. This mainly appears to be a result of the machining process removing portions of the defects and the resulting proximity to the free surface increasing the stress intensity factor. Thus, for a sub-surface defect to initiate a crack, the size of the defect required would be expected to be much larger than one at the surface.

Using the $\sqrt{area}$ approach the stress intensity factor was calculated for each defect. The resulting K_{max} vs cycles to failure is shown in Figure 4 where the solid data points represent defects determined to be sub-surface and the hollow data points determined to be surface defects. While results using this method have been successful in reducing the scatter observed in fatigue data of materials with defects [12], the estimated K_{max} overestimates the effect of the subsurface defects. Figure 4 shows that the effect of K_{max} on the fatigue life for most of the sub-surface and all of the G1_81 data points is over predicted.

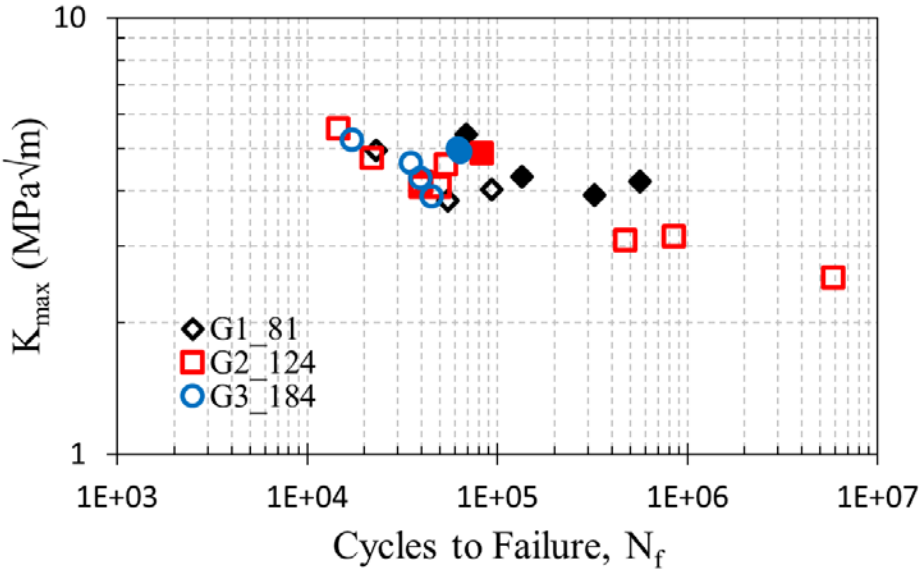

Figure 4: K_{max} estimated using the √area approach and plotted vs fatigue life.

The cause of the overestimation of K_{max} is believed to result from fact that the shape factor Y does not differentiate between defects that are located much further from the surface, as observed for many specimens in G1_81. Typically fatigue cracks initiate much closer to the surface than what was observed for G1_81 specimens, especially in the low life fatigue regime. To overcome the overestimation of K_{max} for sub-surface defects, a new approach was implemented in which the location of the defect was given more weight in the estimation of K_{max}. A dimensionless location ratio in relation to the specimen diameter is calculated and used to modify the equation of K_{max} as shown in Equation 2. Here l is the closest distance from the defect center to the specimen surface and d is the diameter of the specimen. This modified equation now weights the K_{max} term based on the location of the initiating defect. The K_{max} calculated from this modified approach is plotted against fatigue life and shown in Figure 5. It can be seen from this figure that the stress intensity factor is no longer overestimated for the sub-surface defects of G1_81. Additionally, the method does not significantly affect defects that are near the surface as is the case for the solid data points for G2_123 and G3_184 in Figures 4 and 5.

$$K_{max} = \left(\frac{d-l}{d}\right) Y \sigma_{max} \sqrt{\pi \sqrt{area}} \qquad (2)$$

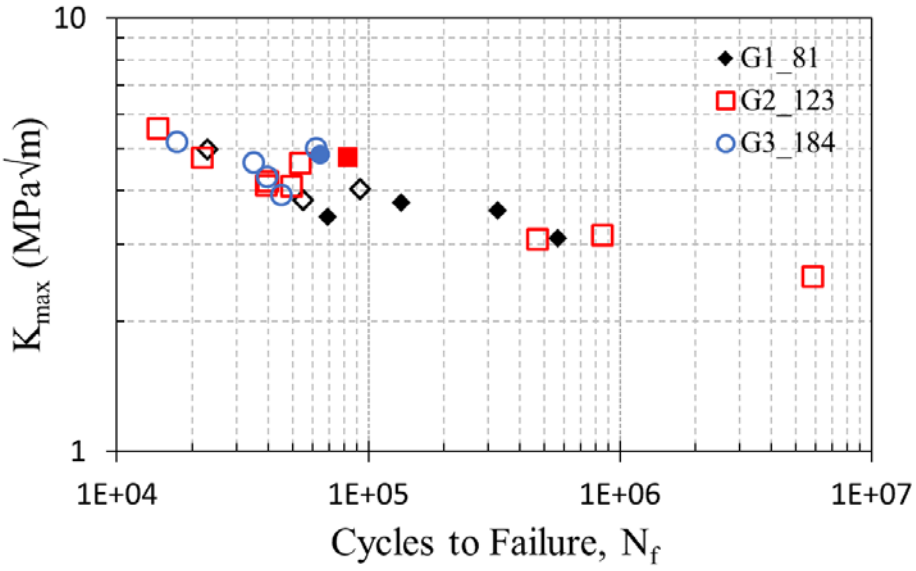

Figure 5: K_{max} based on an equivalent surface defect approach.

The predicted fatigue life using effective surface defect approach vs the observed fatigue life for all tested samples is given in Figure 6. The effective surface defect approach shows acceptable correlation, with all but a single data point falling within a scatter band of four. While the Basquin curves indicate that the fatigue behavior may show some sensitivity to gage volume, the defect analysis provided using the surface defect approach shows that this is due to the defect size and more importantly the location of the defect in relation to the surface. While the location of the defect may be sensitive to gage volume, further research is required to better understand the

defect distribution for various sized parts. The work presented in this study suggest, however, that understanding defect sizes and locations for a given part can lead to improvements in fatigue life estimation and greater confidence for use in structural applications.

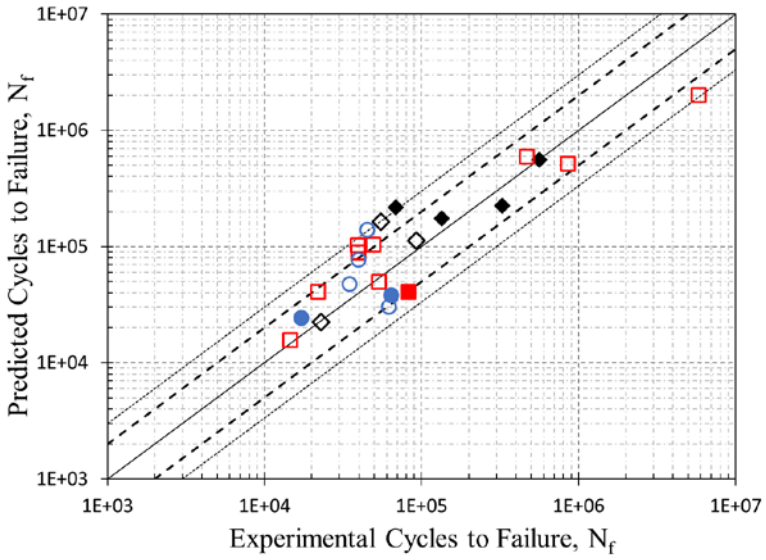

Figure 6: Predicted cycles to failure compared to observed cycles to failure with dotted lines representing a scatter band of 4.

Conclusions

Results show that L-PBF Ti-6Al-4V in the machined and polished condition shows some sensitivity to gage volume. Lower gage volume samples were shown to preferentially initiate cracks at sub-surface defects. This shift in crack initiation behavior is accompanied by an observed improvement in the fatigue life. The Murakami approach of estimating the fatigue life based on the maximum stress intensity factor for the crack initiation defects was shown to overestimate the stress intensity factor for these sub-surface defects. The overestimation of K_{max} is more severe for defects further away from the surface of the specimen. However, using a defect distance to diameter ratio, the modified Murakami $\sqrt{area}$ approach did show acceptable correlation to the data.

Acknowledgements

Partial funding for this work was provided by the National Science Foundation under Grant No. 1657195. Supports from the Naval Air Systems Command (NAVAIR) is also greatly appreciated. Authors also acknowledge the support of Mohammad Masoomi from Auburn University for performing all the simulations of this study.

References

[1] W. Weibull, “A statistical theory of strength of materials,” *IVB-Handl*, 1939.

[2] C. E. Phillips and R. B. Heywood, “The Size Effect in Fatigue of Plain and Notched Steel Specimens Loaded under Reversed Direct Stress,” *Proc. Inst. Mech. Eng.*, vol. 165, no. 1, pp. 113–124, Jun. 1951.

[3] J. Pegues, M. Roach, R. Williamson, and N. Shamsaei, “Surface Roughness Effects on the Fatigue Strength of Additively Manufactured Ti-6Al-4V,” *Int. J. Fatigue*, Accepted 2018.

[4] D. Greitemeier, C. D. Donne, F. Syassen, J. Eufinger, and T. Melz, “Effect of surface roughness on fatigue performance of additive manufactured Ti–6Al–4V,” *Mater. Sci. Technol.*, vol. 32, no. 7, pp. 629–634, May 2016.

[5] A. Yadollahi and N. Shamsaei, “Additive manufacturing of fatigue resistant materials: Challenges and opportunities,” *Int. J. Fatigue*, vol. 98, pp. 14–31, May 2017.

[6] S. Leuders *et al.*, “On the mechanical behaviour of titanium alloy TiAl6V4 manufactured by selective laser melting: Fatigue resistance and crack growth performance,” *Int. J. Fatigue*, vol. 48, pp. 300–307, Mar. 2013.

[7] Q. C. Liu, J. Elambasseril, S. J. Sun, M. Leary, M. Brandt, and P. K. Sharp, “The Effect of Manufacturing Defects on the Fatigue Behaviour of Ti-6Al-4V Specimens Fabricated Using Selective Laser Melting,” *Advanced Materials Research*, 2014. [Online]. Available: https://www.scientific.net/AMR.891-892.1519. [Accessed: 02-Jul-2018].

[8] E. Wycisk, A. Solbach, S. Siddique, D. Herzog, F. Walther, and C. Emmelmann, “Effects of Defects in Laser Additive Manufactured Ti-6Al-4V on Fatigue Properties,” *Phys. Procedia*, vol. 56, pp. 371–378, Jan. 2014.

[9] Y. Murakami and M. Endo, “Effects of defects, inclusions and inhomogeneities on fatigue strength,” *Int. J. Fatigue*, vol. 16, no. 3, pp. 163–182, Apr. 1994.

[10] Y. Murakami and M. Endo, “Effects of Hardness and Crack Geometries on Delta K sub th of Small Cracks Emanating From Small Defects,” *Mech. Eng. Publ. Behav. Short Fatigue Cracks*, pp. 275–293, 1986.

[11] Y. Murakami and M. Endo, “Quantitative evaluation of fatigue strength of metals containing various small defects or cracks,” *Eng. Fract. Mech.*, vol. 17, no. 1, pp. 1–15, Jan. 1983.

[12] S. Beretta and Y. Murakami, “Statistical Analysis of Defects for Fatigue Strength Prediction and Quality Control of Materials,” *Fatigue Fract. Eng. Mater. Struct.*, vol. 21, no. 9, pp. 1049–1065.